Gold Nanorods as Photothermal Antibacterial Materials

ACS APPLIED NANO MATERIALS

www.acsanm.org

Article

Gold Nanorods as Photothermal Antibacterial Materials

Maja Uusitalo, Gustav Eriksson, Mats Hulander, and Martin Andersson*

Cite This: ACS Appl. Nano Mater. 2025, 8, 3661−3670

Read Online

ACCESS | Metrics & More | Article Recommendations | Supporting Information

ABSTRACT: Biomaterial-associated infections (BAIs) are a considerable challenge in modern medicine, limiting the use of many important medical devices and causing severe patient discomfort as well as high societal costs. The reduced susceptibility of biofilm-forming bacteria to antibiotics, along with the increased occurrence of antimicrobial resistant pathogens, have incited an interest in the development of antibacterial biomaterial modifications that can combat BAIs. In the present work, we have developed a biomaterial modification strategy using surface-immobilized photothermal gold nanorods (AuNRs). AuNRs were immobilized on glass and titanium substrates with well-defined surface coverage of 12−14%, leaving most of the substrate surface unmodified. The antibacterial activity of the AuNR-functionalized materials against *Staphylococcus aureus* and *Escherichia coli* was evaluated after irradiation with a near-infrared (NIR) laser (808 nm) at different laser intensities. The AuNR-functionalized glass demonstrated prominent light intensity dependent antibacterial activity upon NIR irradiation, caused by plasmonic heating of the AuNRs, against both *S. aureus* and *E. coli*. In contrast, on titanium the NIR light-induced thermal antibacterial activity was attributed to light absorption by the substrate itself, with no significant effect from the AuNRs. This study provides valuable insights into the role of the substrate properties in developing antibacterial biomaterial modifications using gold nanorods and NIR light, and it furthermore demonstrates the potential of using these systems in combatting BAIs.

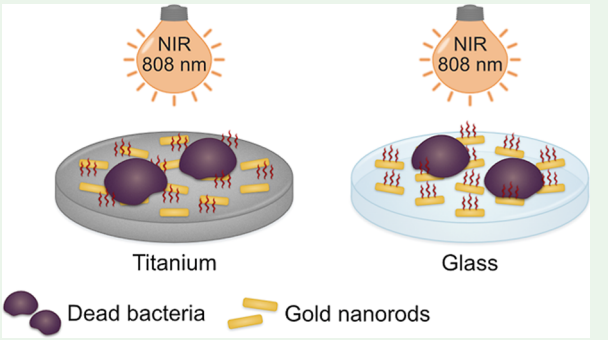

KEYWORDS: *biomaterial-associated infections, photothermal therapy, gold nanorods, near-infrared light, antimicrobial*

INTRODUCTION

Medical implants have widespread use in medicine, providing essential functions for therapeutic, prosthetic, and diagnostic purposes. The demand for medical implants has seen a consistent increase over the recent decades, a trend commonly attributed to a collective effect of advancements within healthcare and demographic changes.[1,2] The increase in demand is predicted to continue, with the number of hip implants used expected to rise by 50% between 2015 and 2050[3] serving as an example. Although medical implants have a crucial role in modern medicine and the current use is widespread, their usage is not without concerns. Biomaterial-associated infections (BAIs), caused by bacterial colonization and subsequent biofilm formation on the biomaterial surface, remain a major challenge with occurrences ranging from 1 to 2%[1] for hip and knee prostheses, and up to 30% for indwelling urinary catheters.[4,5] Once a BAI is established, common treatments include administration of high doses of antibiotics and, when applicable, revision surgery with debridement or complete removal of the implant.[1] In addition to severe discomfort for the patient and high societal costs, the risk of reinfection after revision surgery is considerable.[6,7]

Current prevention strategies for BAIs include aseptic protocols during surgery, as well as pre- and postsurgical administration of antibiotics. Although antibiotics are essential for infection prevention and treatment, the reduced susceptibility of biofilm-forming bacteria to conventional antibiotics, together with the increased occurrence of antibiotic resistant pathogens, strongly limit their effectiveness.[8,9] The need for novel strategies in combating BAIs has led to a great research interest in the development of antibacterial biomaterial modifications. Various approaches have been employed, and they can broadly be divided into contact-killing surfaces, nonadhesive (antifouling) surfaces, drug-eluting materials, or a combination of the above.[5]

One promising approach is the use of gold nanoparticles as photothermal therapy agents.[10] Gold nanoparticles are commonly used for biomedical applications because of their tunable optical properties[11] and low toxicity potential.[12−14] Due to localized surface plasmon resonance (LSPR), plasmonic gold nanoparticles generate heat when exposed to resonant light. For rod-shaped gold nanoparticles, the longitudinal plasmon resonance frequency is shifted from the

Received: January 16, 2025
Revised: January 27, 2025
Accepted: January 31, 2025
Published: February 6, 2025

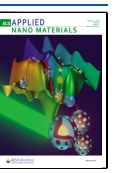

visible to the near-infrared (NIR) region.[11] The possibility to tune the resonance of gold nanorods to wavelengths in the NIR region makes them an excellent candidate for photothermal therapy applications, as this spectral region exhibits optimal tissue penetration due to minimum absorption by water and hemoglobin.[15]

Gold nanorods in suspension have previously been studied for photothermal therapy (PTT) of both cancer[10,16,17] and bacterial infections.[18,19] However, when relying on systemic administration, suspended particles present challenges such as colloidal stability and target specificity for *in vivo* use. By immobilizing the gold nanorods on a biomaterial surface, a light-activated, local, and broad-spectrum antibacterial modification for combating BAIs can be realized. The concept of utilizing the photothermal properties of surface-immobilized gold nanorods to develop antibacterial biomaterials has been investigated on several materials, including titanium,[20] glass,[21,22] polypropylene,[23] polyurethane,[24,25] and polyacrylonitrile.[26] While previous research on using these systems to eradicate bacteria shows promise, limitations such as extensive material preparation protocols and need of high surface coverage of nanoparticles remain to be addressed. Furthermore, it is of interest to understand the factors affecting the antibacterial activity of the materials.

The present study demonstrates straightforward and reproducible procedures for the surface-immobilization of gold nanorods. Utilizing electrostatic interactions, the procedures achieved well-defined and discrete nanoparticle placement on both glass and titanium surfaces. The surface-immobilization was characterized with Vis-NIR spectroscopy, scanning electron microscopy (SEM) and X-ray photoelectron spectroscopy (XPS), showing successful gold nanorod-functionalization of both materials. The antibacterial activity of the materials upon illumination with a NIR laser (808 nm) was evaluated against *Staphylococcus aureus*, a common pathogen found in BAIs,[6] and *Escherichia coli*, a species frequently causing catheter-associated urinary tract infections.[27] The *in vitro* evaluation revealed that the antibacterial activity exhibited a clear dependency on the NIR light intensity, and furthermore showed discrepancies in the origin of the antibacterial effect between glass and titanium. The findings present a new approach for the surface-immobilization of gold nanorods, and highlight the importance of the underlying substrate for the photothermal antibacterial activity of the gold nanorod-functionalized materials upon exposure to NIR light.

EXPERIMENTAL SECTION

Unless otherwise stated, all chemicals were purchased from Sigma-Aldrich Sweden AB and used without further modification. Glassware for the AuNR synthesis and surface-immobilization was cleaned with a basic piranha solution prepared by mixing ultrapure water (Milli-Q, 18.2 MΩ·cm, Merck Millipore), ammonia solution (28%, VWR) and hydrogen peroxide (30%, Fisher Scientific) in a 5:1:1 ratio and heating it to 70 °C. After cleaning, the glassware was rinsed thoroughly with ultrapure water and dried with nitrogen gas. The near-infrared laser used in this work was acquired from BWT Beijing Ltd., having a central wavelength of 808 ± 3 nm (model DS3-51523-50.00W). The laser was connected to an air-spaced doublet collimator (F810SMA-780, Thorlabs) and a 2X beam expander (GBE02-B, Thorlabs). The irradiance output from the laser system was measured using an optical power meter (Thorlabs, PM160T-HP), data are shown in the Supporting Information (Figure S1 and Table S1).

Gold Nanorod Synthesis. The gold nanorod synthesis was adapted from a seed-mediated procedure described elsewhere.[28] In brief, a seed suspension was prepared in a 30 °C water bath by adding 25 μL of 50 mM gold(III) chloride ($HAuCl_4$) solution to 4.7 mL of 100 mM hexadecyltrimethylammonium bromide (CTAB) solution. Thereafter, 300 μL of 10 mM sodium borohydride was added under strong stirring. The resulting seed suspension was kept mildly stirring at 30 °C until use. A growth solution was prepared in a 30 °C water bath by adding 1.14 mL of 1 M HCl and 600 μL of 50 mM $HAuCl_4$ to 60 mL of 100 mM CTAB solution. Next, 720 μL of 10 mM silver nitrate was added, followed by 600 μL of 100 mM ascorbic acid, producing a colorless growth solution. Lastly, 144 μL of the seed suspension was added to the growth solution, thoroughly mixed, and left undisturbed at 30 °C for 1 h and 50 min. The synthesized AuNRs were centrifuged and redispersed in ultrapure water three times. A detailed protocol for the purification is available in the Supporting Information. The final suspension of AuNRs dispersed in ultrapure water was used as stock in the surface-immobilization procedures.

Preparation of Gold Nanorod-Functionalized Substrates. The functionalization protocols were based on electrostatic immobilization of the positively charged CTAB-stabilized AuNRs on negatively charged substrate surfaces. The substrates included glass (round coverslips, #1.5, ⌀13 mm, VWR) and titanium (discs, 2 mm thickness, ⌀9 mm). The study was limited to two substrate materials, where glass was chosen due to its suitable optical properties, and titanium as a material commonly used for medical implants. Both substrates were rinsed with 95% ethanol (Solveco AB) followed by ultrapure water before being dried with nitrogen gas. Thereafter, the substrates were pretreated using different approaches depending on the material, to obtain clean and negatively charged surfaces. The glass coverslips were placed in a glass Petri dish, covered with nitric acid (65−67%) and left overnight (18−19 h). After acid pretreatment, the coverslips were rinsed thoroughly with ultrapure water before being immersed in an aqueous AuNR suspension for 5 h. The titanium discs were pretreated in an UV/O_3 cleaner for 15 min, and thereafter immersed in an aqueous AuNR suspension for 5 h.

The AuNR suspensions used for the surface-immobilization was prepared by diluting the stock AuNR with ultrapure water to an absorbance at 400 nm of 0.35, which was estimated to a gold concentration of 30 μg/mL based on a method described elsewhere.[28] An absorption spectrum of the AuNR suspension used for the surface-immobilization (Figure S2) and the calculation of the estimated gold concentration is available in the Supporting Information. After the 5 h immersion, the AuNR suspension surrounding the substrates was exchanged to ultrapure water. Lastly, the substrates were immersed in 99.5% ethanol (Solveco AB) and left to air-dry, producing the final AuNR-functionalized glass (Glass-AuNR) and titanium (Ti-AuNR) samples.

Material Characterization. *Transmission Electron Microscopy.* Transmission Electron Microscopy (TEM) samples were prepared by placing 5 μL AuNR suspension (diluted 1:29 from the stock) on UV/O_3-treated copper grids with an ultrathin carbon film on a lacey carbon support film (TED Pella). Excess suspension was removed by blotting the grid with filter paper. TEM analysis was performed using a FEI Titan 80−300 operated in TEM mode at 300 kV. The acquired micrographs were analyzed using Gatan Microscopy Suite 3. The AuNR dimensions (length, width, aspect ratio) were determined from TEM micrographs using the image analysis software Fiji (ImageJ). A total of 300 nanoparticles were measured.

Electrophoretic and Dynamic Light Scattering. Electrophoretic and dynamic light scattering (ELS and DLS) were performed using a Litesizer DLS 500 from Anton Paar. The stock AuNR suspension was diluted (1:49) to an estimated gold concentration of 15 μg/mL with ultrapure water and the measurements were performed at 25 °C. The measurement angle used for DLS was 175° (backscatter) and both ELS and DLS measurements were repeated three times.

Vis-NIR Spectroscopy. Vis-NIR spectroscopy was performed using a Multiskan GO Microplate Spectrophotometer from Thermo Scientific. The plasmonic properties of the AuNRs in suspension and the optical properties of the Glass-AuNR immersed in water were

https://doi.org/10.1021/acsanm.5c00324
ACS Appl. Nano Mater. 2025, 8, 3661−3670

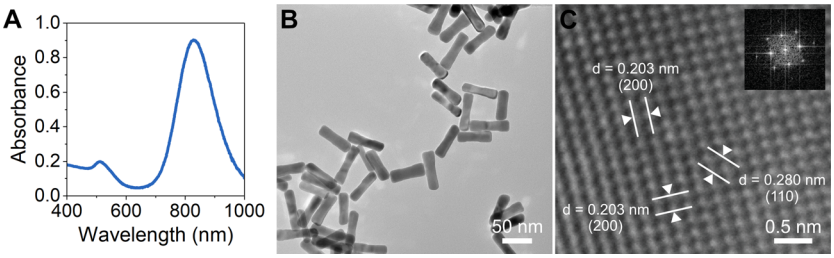

Figure 1. Gold nanorod characterization. (A) Vis-NIR absorption spectrum of the synthesized gold nanorods. (B) Overview and (C) high-resolution TEM micrographs of gold nanorods.

characterized by measuring the absorption spectra between 400 and 1000 nm.

Scanning Electron Microscopy. The AuNR surface-immobilization was characterized using a Zeiss Ultra 55 scanning electron microscope. Glass-AuNR and Ti-AuNR samples were imaged in secondary electron mode with acceleration voltages of 2−5 kV. Micrographs were analyzed with respect to surface coverage (projected area covered by AuNRs). Thresholding was performed using Otsu's method, implemented in Python. For the determination of surface coverage from scanning electron microscopy (SEM) micrographs, six Glass-AuNR and six Ti-AuNR ($N = 6$) samples were analyzed. For each sample, nine micrographs acquired at different locations distributed across the entire sample were used.

Scanning electron microscopy was further used to study the bacteria−material interaction on the samples from the *in vitro* antibacterial activity evaluation. Samples were removed from the agar plates after colony counting and immersed in 4% formaldehyde (VWR) for 90 min. Thereafter the samples were dehydrated by stepwise immersion in an ethanol gradient (20, 40, 60, 80, 100% v/v in water) with 10 min immersion per step. After dehydration, the samples were transferred to a solution of 50% v/v hexamethyldisilazane (HDMS) in ethanol and left for 15 min. Lastly, a final immersion in 100% HDMS for 15 min was performed before the samples were air-dried. Prior to SEM characterization, the samples were sputter coated with approximately 5 nm of gold.

X-ray Photoelectron Spectroscopy. X-ray Photoelectron Spectroscopy (XPS) was used to characterize the surface elemental composition of the AuNR-functionalized glass and titanium. Glass-AuNR and Ti-AuNR samples were examined before and after UV/O_3-treatment for 5 min. The UV/O_3-treatment was conducted to sterilize the samples prior to the *in vitro* antibacterial activity evaluation. XPS was performed using a Versaprobe III spectrometer (PHI) with monochromated Al Kα radiation for excitation. The spot size illuminated by the X-ray beam was 100 × 100 μm and spectra were recorded with a 45° takeoff angle. Survey spectra were measured with 224 eV pass energy and a step-size of 0.4 eV with 20 ms dwell time per data point and 4 accumulated sweeps. Detailed spectra of the core levels were measured with 26 eV pass energy and a step-size of 0.05 eV (Au 4*f*, C 1*s*) or 0.1 eV (Ag 3d, Br 3d). Sample charging was compensated for using an electron flood gun and an Ar^+ ion source. Recorded spectra were normalized to the background at the low binding energy side. The binding energy scale was referenced to the Ti $2p_{3/2}$ signal for the titanium samples. The main Ti 2p line was assumed to originate from a TiO_2 overlayer with its $2p_{3/2}$ signal positioned at 459.3 eV.[29] The position of the C 1*s* signal is not a reliable reference point, especially when making relative comparisons for samples on different supports.[30] Hence, the Au 4f signals for the AuNRs on glass were shifted to match the signal from the titanium samples. Relative quantification of the elements was done with the Multipak software (PHI). The integral intensity of the signals was evaluated and corrected with atomic sensitivity factors.

Thermal Imaging. The macroscopic heating of the Glass-AuNR and Ti-AuNR upon irradiation with the NIR laser was evaluated through thermal imaging of the samples using a testo 871s thermal imager. The samples were placed onto brain heart infusion (BHI) agar plates with the AuNRs facing the agar and thereafter irradiated through the bottom of the agar plates, with the laser collimator placed at a 60° angle relative to the sample surface. Thermal images were taken before and after 30 s NIR irradiation. Nonfunctionalized glass and titanium substrates were used as control. The measurements were performed two times.

In Vitro Antibacterial Activity. The microorganisms used for the *in vitro* antibacterial activity evaluation were *S. aureus* (CCUG 10778) and *E. coli* (CCUG 29300T). For long-term storage the bacteria were kept at −80 °C. The bacteria were spread on BHI agar to form single colonies, and the plates were used within one week. All samples used in the *in vitro* studies were sterilized by exposure to UV light for 5 min in a UV−O_3 cleaner. The antibacterial activity was evaluated using an agar plate model. *S. aureus* or *E. coli* was inoculated in tryptic soy broth (TSB) and incubated at 37 °C until it reached approximately 10^8 CFU/mL, determined by measuring the optical density (Biowave CO8000 Cell Density Meter, Biochrom WPA). The bacterial suspension of *S. aureus* was diluted to approximately 5 × 10^4 CFU/mL with phosphate buffered saline (PBS), and the suspension of *E. coli* to approximately 1 × 10^4 CFU/mL, whereafter the suspensions were streaked onto BHI agar plates using cotton swabs. The bacterial concentrations were optimized for the experimental protocol used to evaluate the antibacterial surfaces (a two-dimensional system). This optimization explains why a lower concentration was used compared to the 5 × 10^5 CFU/mL applied in the broth dilution method for determining minimum inhibitory concentration (MIC) of antimicrobial compounds in suspension (a three-dimensional system).

Four samples were randomly placed onto each agar plate. The AuNR-functionalized side of the samples was placed facing the bacteria/agar. Nonfunctionalized glass and titanium substrates were used as controls. The antibacterial activity was evaluated as a function of NIR light intensity, and as such, only one irradiation time (30 s) was assessed.

The antibacterial activity of the gold nanorod-functionalized titanium was evaluated against *S. aureus*. Ti-AuNR and control samples on the agar plates were irradiated with the NIR laser for 30 s using two different irradiances: 5 and 10 W/cm^2. As the titanium substrates are not transparent to the NIR light, they were irradiated through the bottom of the agar plates. A schematic of the experimental setup is shown in the Supporting Information (Figure S3A). The antibacterial activity of the gold nanorod-functionalized glass was evaluated against *S. aureus* and *E. coli*. For *S. aureus*, Glass-AuNR and control samples on the agar plates were irradiated with the NIR laser for 30 s using three different irradiances: 5, 10, and 20 W/cm^2. For *E. coli*, Glass-AuNR and control samples on the agar plates were irradiated with the NIR laser for 30 s using an irradiance of 20 W/cm^2. The glass samples were irradiated through the back, a schematic of the experimental setup is shown in Supporting Information (Figure S3B). The irradiation order of the samples was randomized. After irradiation, the agar plates were incubated at 37 °C for 16 h, whereafter the bacterial colonies on each sample were counted. To avoid growth from the perimeter of the samples to influence the quantification, colonies on the outmost 1 mm of the samples were excluded. The antibacterial efficacy (in percent) was calculated as $(A - B)/A \times 100$, where A is the number bacterial colonies per unit area (CFU/cm^2) of the control group, and B the number of colonies per unit area of the test group.

https://doi.org/10.1021/acsanm.5c00324
ACS Appl. Nano Mater. 2025, 8, 3661−3670

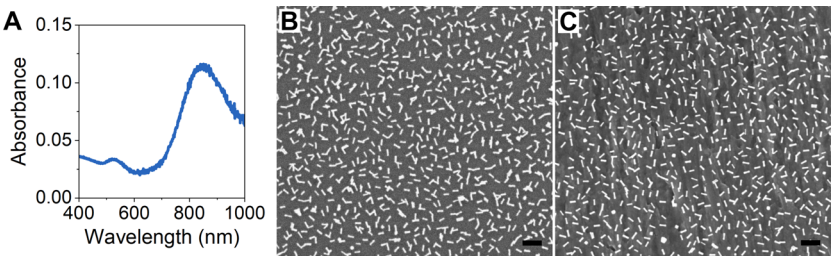

Figure 2. Characterization of gold nanorod-functionalized materials. (A) Vis-NIR absorption spectrum of gold nanorod-functionalized glass (Glass-AuNR) immersed in water. SEM micrographs of gold nanorod-functionalized (B) glass (Glass-AuNR) and (C) titanium (Ti-AuNR). The scale bars are 200 nm.

Statistical Analysis. For the *in vitro* antibacterial activity evaluation, all sample groups were run in triplicates and the experiments were performed three times ($N = 9$). Results for each sample group were expressed as average CFU/cm^2 values, and standard deviations were used to indicate distribution around the means. Significance testing was performed using pairwise two-sample *t*-test assuming unequal variances. Significant differences in bar charts are indicated with letters. Two groups with the same letter indicate that there is no statistically significant difference between the means, two groups with different letters indicate that there is a statistically significant difference between the means.

RESULTS AND DISCUSSION

Gold Nanorod Characterization. The absorption spectrum of the synthesized gold nanorods in Figure 1A exhibits a transverse surface plasmon resonance band at 500−550 nm and a longitudinal band in the NIR region with a maximum at 825 nm. The high relative intensity of the longitudinal band compared to the transverse indicates a high shape purity of the synthesized nanorods,[31] and the narrow width of the longitudinal band a low size dispersion.[28] Figure 1B shows an overview TEM micrograph of the AuNR morphology and Figure 1C a high-resolution TEM (HRTEM) micrograph with a FFT insert, highlighting the fcc single-crystalline nature of the AuNRs. The lattice fringes observable in Figure 1C have distances in good agreement with the lattice spacing of the (200) planes in gold (0.203 nm) perpendicular to and in parallel with the growth direction of the nanorod. Distances in acceptable agreement with the (110) planes in gold (0.287 nm) are also notable. A lower magnification TEM micrograph showing the location of the HRTEM micrograph in Figure 1C in relation to the growth direction of the nanorod is included in the Supporting Information (Figure S4). Overall, the observed crystal structure of the AuNRs agrees well with literature regarding gold nanorods synthesized in the presence of silver.[32]

The AuNRs had a length of 67 ± 7 nm, a width of 18 ± 2 nm, and an aspect ratio of 3.9 ± 0.5. Histograms showing the distribution of the AuNR dimensions are included in the Supporting Information (Figure S5). The electrophoretic mobility of the AuNRs was determined to be 4.12 ± 0.07 μm·cm/(V s), from which the average zeta potential was calculated to 52.9 mV using the Smoluchowski approximation. Details on the DLS measurements and results are included in the Supporting Information (Figure S6). The DLS results were not used as a metric of particle size due to the limitations of DLS for nonspherical particles.

The AuNR aspect ratio was chosen to give a longitudinal LSPR band matching the 808 nm laser. Although it is possible to achieve the desired aspect ratio with other dimensions of AuNRs than the ones used in this work, no evaluation of how the AuNR size influences the antibacterial activity was conducted. A previous study of AuNRs on glass has shown that the surface coverage on the support, rather than the exact dimensions of the AuNRs, has a greater influence on the temperature achieved upon NIR irradiation, through collective heating effects.[33] By extension, the photothermal antibacterial activity of the systems is also expected to depend primarily on the surface coverage rather than the exact AuNR dimensions.

Characterization of Gold Nanorod-Functionalized Materials. Performing Vis-NIR spectroscopy on the AuNR-functionalized glass immersed in water revealed that the particles retained their plasmonic properties once immobilized on glass (Figure 2A). The electrostatic immobilization procedures yielded even and well-defined coverage of AuNRs on both the glass (Figure 2B) and the titanium (Figure 2C) substrates, without formation of larger aggregates. The surface coverage (projected area) of AuNRs on glass was 13.7 ± 1.3%, which, using the average dimensions of the AuNRs, corresponded to 113 ± 10 AuNR/μm^2. For the titanium, the surface coverage was 11.7 ± 0.9%, corresponding to 97 ± 8 AuNR/μm^2. Additional SEM micrographs of the AuNR-functionalized glass and titanium are included in Supporting Information (Figure S7).

Previously published protocols for the surface-immobilization of AuNRs include cleaning and/or pretreatment of the substrate followed by functionalization with linking molecules like (3-mercaptopropyl)trimethoxysilane (MPTMS),[21,22,24,25] aminopropyltrimethoxysilane (APTES) followed by polystyrenesulfonate (PSS),[20] or ethylene diamine,[23] before attachment of the AuNRs. With the straightforward procedures developed here, utilizing electrostatic interaction between the cationic AuNRs and an anionic substrate surface, we have shown that successful and reproducible AuNR-functionalization can be achieved on glass and titanium (Figure 2B,C) without the requirement of linking agents. However, this is only achievable if suitable pretreatment of the substrate is conducted. Avoiding the use of linking agents is beneficial for retaining the often-desired surface chemistry of the biomaterials, and for simplifying material preparation protocols.

For titanium, activation by UV/O_3-treatment was sufficient for obtaining the desired negative surface charge. For glass, however, the choice of preconditioning was shown to be of high importance. Multiple procedures were evaluated before the final protocol using immersion in nitric acid was established, including functionalization with MPTMS, and pretreating the glass with basic piranha solution, with UV/O_3, and with oxygen plasma. Neither yielded functionalization as even and reproducible as the HNO_3 pretreatment, which has been shown to reduce the amount of sodium, calcium, and aluminum cations on the surface of the glass,[34] leaving behind

https://doi.org/10.1021/acsanm.5c00324
ACS Appl. Nano Mater. 2025, 8, 3661−3670

a highly negatively charged surface to which the cationic AuNRs readily attach. The strategy employed here, of utilizing electrostatic interaction to surface-immobilize AuNRs, is feasible to extend to various materials for which it is possible to obtain a hydroxylated surface, e.g. certain metals, ceramics, bioglasses, and polymers. The general nature of the modification strategy thus makes it potentially suitable for a range of biomaterial applications.

Survey and detailed XPS spectra were obtained to characterize the surface elemental composition of Glass-AuNR and Ti-AuNR, both untreated and after UV/O_3-treatment (Supporting Information, Figure S8). Quantification of the atomic concentrations on the sample surfaces, shown in Table 1, confirmed that the AuNRs constituted only a minor

Table 1. Surface Chemical Composition in Atomic Percent Determined with XPS for Glass-AuNR and Ti-AuNR, Untreated and after UV/O_3-Treatment

	atomic concentration %						
	C 1s	O 1s	Si 2p	Ti 2p	Br 3d	Ag 3d	Au 4f
Glass-AuNR	10.6	62.0	22.5		0.31	0.82	3.75
Glass-AuNR UV/O_3	7.1	64.3	23.8		0.29	0.80	3.75
Ti-AuNR	23.5	53.7		17.2	0.37	0.97	4.31
Ti-AuNR UV/O_3	16.1	59.4		19.7	0.29	0.87	3.75

portion of the surfaces. This finding, also evident from SEM characterization (Figure 2B,C), was indicated by the low atomic percentages of gold and silver present. As the AuNR-functionalization resulted in only minor alteration to the surface chemical composition of the substrate, it shows promise as an antibacterial modification strategy that minimizes impact on the biomaterial's surface chemistry.

XPS furthermore revealed that the UV/O_3-treatment resulted in a reduction in the carbon content of the samples (Table 1), indicating removal of hexadecyltrimethylammonium cations from CTAB remaining on the surface-immobilized AuNRs. CTAB alone is toxic to cells at submicromolar concentrations, and although studies have shown that CTAB adsorbed onto gold nanoparticles have limited impact on cell viability,[13,35] its removal from the materials remains important to promote biocompatibility.

To evaluate the macroscopic heating of the titanium and the glass samples upon NIR irradiation, thermal images were obtained before and after irradiating the samples for 30 s while placed on agar plates. The temperature increase for three different irradiances (5, 10, and 20 W/cm^2) was determined as the difference in temperature at the center of the samples before and after irradiation, with the starting temperature ranging between 24 and 25 °C. The average temperature difference for the two replicates of each sample type is shown in Figure 3. The raw data and example thermal images taken after irradiation are included in Supporting Information (Table S3, Figures S9 and S10).

The Ti and Ti-AuNR exhibited a comparable temperature increase with irradiance (Figure 3A), both increasing around 28 °C after 30 s irradiation at 20 W/cm^2, which was enough to melt the agar in contact with the sample surfaces. In contrast, there was a difference in the temperature increase with irradiance between the Glass and Glass-AuNR, wherein the Glass-AuNR increased approximately 17 °C after 30 s

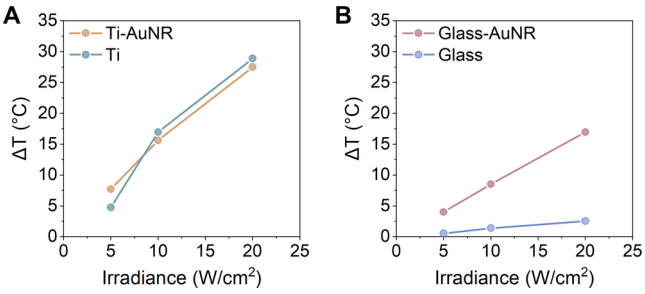

Figure 3. Temperature increase (ΔT) as a function of NIR laser irradiance determined from thermal imaging, for (A) Ti and Ti-AuNR, and (B) Glass and Glass-AuNR. The thermal imaging was conducted with the samples placed on BHI agar plates, and the temperature increase was determined as the difference in temperature at the center of the samples before and after 30 s NIR irradiation.

irradiation at 20 W/cm^2, compared to barely 3 °C for the Glass. As such, the influence from the photothermal heating of the AuNRs was greater when using glass as the support compared to titanium.

***In Vitro* Antibacterial Activity.** The antibacterial activity of the AuNR-functionalized titanium and glass was evaluated as a function of the NIR laser intensity for 30 s irradiation time using an agar plate model. Bare titanium (Ti) and glass (Glass) substrates were used as controls.

Gold Nanorod-Functionalized Titanium (Ti-AuNR). A significant antibacterial activity against *S. aureus* was observed for both Ti-AuNR and Ti irradiated at 10 W/cm^2 for 30 s, compared with all other sample groups (Figure 4). As it is

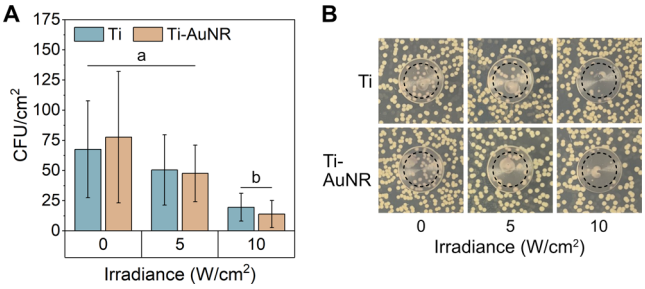

Figure 4. Antibacterial activity against *S. aureus* of Ti-AuNR irradiated with NIR light for 30 s of different irradiances (0 = nonirradiated, 5 and 10 W/cm^2). (A) Data expressed as CFU/cm^2, $N = 9$. Significance level: $p < 0.05$. (B) Showing example pictures of the samples from the agar plate model, bacterial colonies appearing as yellow dots and black dashed lines encircles the sampling area.

preferable to work with as low laser intensities as possible while obtaining an antibacterial effect, the titanium studies were therefore limited to 10 W/cm^2. The Ti-AuNR irradiated at 10 W/cm^2 had an antibacterial efficacy of 82% compared to the nonirradiated Ti-AuNR, and of 79% compared to the nonirradiated Ti (average CFU/cm^2 values compared). The Ti irradiated at 10 W/cm^2 had an antibacterial efficacy of 75% compared to the nonirradiated Ti-AuNR and of 71% compared to the nonirradiated Ti. However, no significant difference in antibacterial activity was observed between the Ti-AuNR and Ti irradiated at 10 W/cm^2 for 30 s, showing that with titanium as the support, no significant effect from photothermal heating of the AuNRs was obtained. The demonstrated antibacterial activity was instead correlated to the laser intensity, where no reduction in bacterial viability was observed at the lower

https://doi.org/10.1021/acsanm.5c00324
ACS Appl. Nano Mater. 2025, 8, 3661−3670

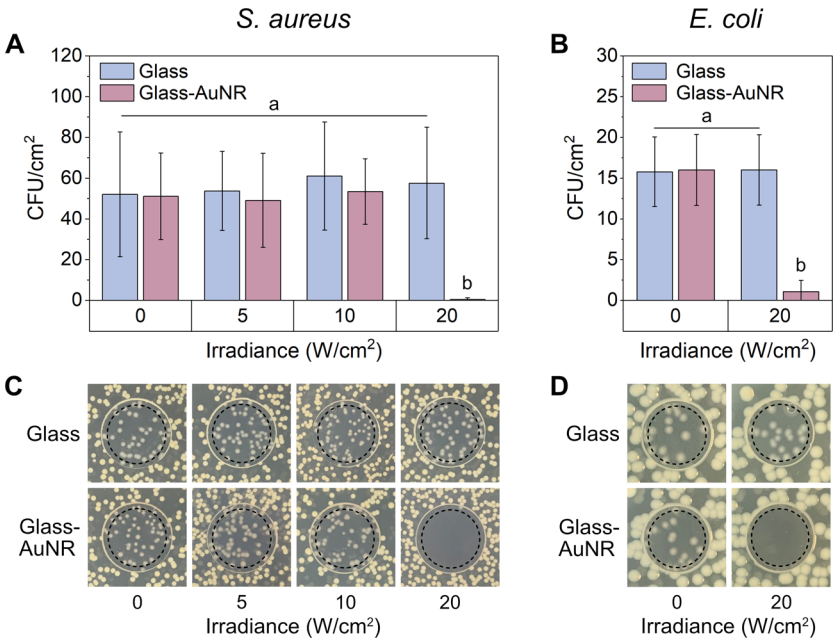

Figure 5. Antibacterial activity of Glass-AuNR irradiated with NIR light for 30 s. (A,C) showing the activity against *S. aureus* for irradiances 0 (nonirradiated), 5, 10, and 20 W/cm^2. (B,D) showing activity against *E. coli* for irradiances 0 (nonirradiated) and 20 W/cm^2. The data presented in (A,B) is expressed as CFU/cm^2, $N = 9$. Significance level: $p < 0.001$. (C,D) show example images from the agar plate model for *S. aureus* and *E. coli*, respectively, with bacterial colonies appearing as yellow dots and black dashed lines encircles the sampling area.

irradiance evaluated (5 W/cm^2), but at a sufficient intensity (10 W/cm^2) a significant reduction occurred for both the Ti-AuNR and Ti. The antibacterial effect could hence be attributed to NIR light absorption by the titanium substrate, which has a high optical extinction coefficient at 808 nm,[36] leading to heating of the samples. These findings align with the thermal imaging, which revealed no obvious difference in temperature increase with laser intensity between the Ti-AuNR and Ti (Figures 3A and S9), and further antibacterial studies on the titanium substrates were therefore not pursued. The lack of effect from photothermal heating of the AuNRs is furthermore supported by the fact that titanium is known to have plasmon damping properties, where the disruption of the plasmon resonance stems from its dielectric function that introduces absorption and influences the refractive index locally.[37,38]

The antibacterial activity of bare titanium upon NIR irradiation has been shown in previous work studying the antibacterial properties of AuNRs on titanium.[20] In contrast to our results, however, the referenced study demonstrated significant antibacterial activity from AuNRs on titanium upon NIR irradiation. This discrepancy can likely be explained by the fact that our study evaluates titanium substrates functionalized with discrete AuNRs at a surface coverage around 12%, whereas the referenced study employed complete multilayer coatings of AuNRs on titanium. It is feasible that by using multilayer coatings of AuNRs, the influence of plasmon damping induced by the titanium substrate could be minimized, however, disadvantages including plasmon coupling between the AuNRs and changing the surface chemistry of the substrate arise. Our results further showed no significant antibacterial activity for the nonirradiated Ti-AuNR (Figure 4A), indicating that the AuNR-functionalization had no influence on bacterial viability. This also contrasts previous work, where the AuNR coating reduced the bacterial viability compared to a noncoated control, an effect that was attributed to the wettability of the coating and silver content in the AuNRs.[20]

The results obtained from the SEM analysis of the titanium samples from the antibacterial activity evaluation against *S. aureus* are included in the Supporting Information (Figures S11 and S12). As a few bacterial colonies were present on the samples that exhibited a significant antibacterial activity (Figure 4B) and the bacterial load thus varied over the samples, SEM characterization did not contribute with representative and complementary information.

Gold Nanorod-Functionalized Glass (Glass-AuNR). From the *in vitro* evaluation against *S. aureus* (Figure 5A,C), the Glass-AuNR demonstrated a significant antibacterial activity when irradiated at 20 W/cm^2 for 30 s, compared to all other sample groups. The Glass-AuNR irradiated at 20 W/cm^2 had an antibacterial efficacy of 99% compared to the nonirradiated Glass-AuNR as well as to the Glass irradiated at 20 W/cm^2 (average CFU/cm^2 values compared). No significant antibacterial effect was observed for the lower irradiances assessed (5 and 10 W/cm^2). To evaluate the antibacterial activity of the Glass-AuNR against Gram-negative bacteria, the irradiation parameters that yielded a significant effect against *S. aureus* (20 W/cm^2, 30 s) were also tested against *E. coli* (Figure 5B,D). The Glass-AuNR irradiated at 20 W/cm^2 for 30 s exhibited a significant antibacterial activity against *E. coli*, compared to all other sample groups. An antibacterial efficacy of 93% was observed compared to the nonirradiated Glass-AuNR as well as the Glass irradiated at 20 W/cm^2 (average CFU/cm^2 values compared). The strong antibacterial activity demonstrated against both *S. aureus* and *E. coli* emphasizes the potential of harnessing the photothermal heating of the AuNRs to achieve a light-activated and broad-spectrum antibacterial surface modification. Furthermore, no significant antibacterial activity was observed for the non-irradiated Glass-AuNR (Figure 5A,B) against either bacterial

https://doi.org/10.1021/acsanm.5c00324
ACS Appl. Nano Mater. 2025, 8, 3661−3670

strain, indicating that the AuNR-functionalization did not affect bacterial viability.

In contrast to the titanium samples, with glass as the support, which is transparent to NIR light, a clear photothermal antibacterial activity from plasmonic heating of the AuNRs was observed. This aligns with the thermal imaging results, where the Glass-AuNR exhibited a steeper temperature increase with laser intensity compared to the Glass (Figures 3B and S10). The discrepancy in the origin of the antibacterial activity between the glass and titanium highlights the important influence of the substrate properties on the bactericidal effect of these systems. To harness the plasmonic heating of the AuNRs, employing the modification strategy on biomaterials with properties like glass, i.e. having low optical extinction in the NIR region, shows greater potential.

Interestingly, for the short irradiation time evaluated (30 s), an irradiance as high as 20 W/cm^2 was required to effectively eradicate bacteria when using glass as the support. It is worth emphasizing that the high laser intensity did not in itself influence bacterial viability, as no significant antibacterial effect was observed for the irradiated glass control samples (Figure 5). Moreover, for the irradiated Glass-AuNR samples where an antibacterial effect was observed, bacteria were able to recolonize the surface from outside the illuminated area (Figure S13). This highlights the local nature of the photothermal antibacterial activity from the AuNRs, showing promise for minimal negative influence on surrounding tissue cells. However, essential *in vitro* studies are still needed to evaluate the effects of the NIR laser, AuNR-functionalization, and photothermal heating on eukaryotic cells.

Whereas this study focused on the laser intensity dependency, previous studies have employed lower laser intensities (0.2 W, 0.5−2 W/cm^2) and assessed the antibacterial effect as a function of longer irradiation times (2−20 min).[20−22,24] As the temperature of the AuNRs depends on the light intensity used for excitation, an interesting aspect is whether the antibacterial effect obtained using a high laser intensity for a short time, as in our work, compared to a lower intensity for longer time, is caused by the same mechanism. In hyperthermia, where the temperature is increased to 40−50 °C for several minutes, cell damage is caused by protein denaturation and cell membrane destruction.[10] However, for gold nanoparticles in an aqueous environment, formation of microscale bubbles can occur if sufficiently high temperatures are reached (>200 °C),[39] which can impose mechanical stress resulting in cell damage.[10] Obtaining a moderate temperature increase for prolonged periods of time to induce hyperthermia, compared to attaining a locally very high temperature, could thus be inducing an antibacterial effect through different mechanisms. Previous work has shown that the temperature of AuNRs supported on glass in an air environment can reach over 100 °C under NIR irradiation at intensities similar to those utilized here.[33] The temperature of the AuNRs is thus likely much higher than the macroscopic temperature increase that was observed during the thermal imaging of the Glass-AuNR samples (Figures 3B and S10). As such, it is possible that hyperthermia is not the only or main antibacterial mechanism for the systems studied in this work. However, to investigate the potentially different mechanisms, further studies of the systems are needed, along with improved insights into the temperature reached by the surface-immobilized AuNRs.

For the SEM analysis of the glass samples from the antibacterial activity evaluation against *S. aureus* (Figure 6),

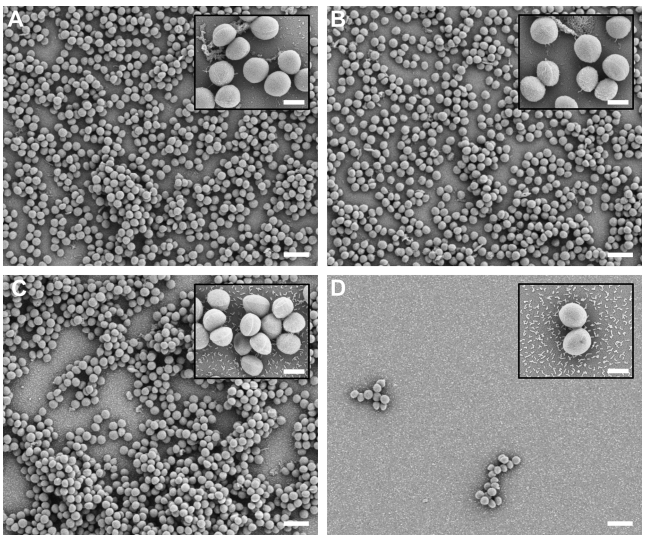

Figure 6. SEM micrographs of samples from the antibacterial activity evaluation of Glass-AuNR against *S. aureus*. The samples shown being (A) Glass, (B) Glass irradiated at 20 W/cm^2 for 30 s, (C) Glass-AuNR, and (D) Glass-AuNR irradiated at 20 W/cm^2 for 30 s. The low and high (insert) magnification scale bars are 2 μm and 500 nm, respectively.

micrographs were taken at the edges of the colonies visible in Figure 5C, where the bacterial count was low enough to visualize the underlying substrate, where applicable. The micrographs in Figure 6A−C for samples Glass, Glass 20 W/cm^2 and Glass-AuNR, respectively, reveal the formation of biofilms on the sample surfaces. On the contrary, for the Glass-AuNR 20 W/cm^2 sample (Figure 6D) no biofilm formation occurred, and only small clusters of bacterial cells could be observed at a few locations. Lower magnification micrographs showing the large difference in bacterial load between the sample groups are included in the Supporting Information (Figure S14). The SEM analysis further revealed the AuNR-functionalization of the glass to be largely unaffected after the antibacterial activity evaluation (inserts in Figure 6C,D). Similarly, the Ti-AuNR samples showed retained AuNR coverage after the *in vitro* antibacterial tests (inserts in Figure S11C,D).

When evaluating the efficacy of an antibacterial biomaterial modification, the choice of *in vitro* model is critical for accurate assessment. Our agar plate model provided an efficient way of quantifying the local antibacterial effect and could serve as a future model for studying bacterial infections in the surrounding tissue of a biomaterial. By seeding bacteria on an agar plate and placing the biomaterial on top of the inoculum, the transfection from tissue to the biomaterial surface is mimicked and could better reflect the onset of a BAI. Upon irradiation with NIR light of sufficient intensity, a significant antibacterial activity was observed for the Glass-AuNR, and bacterial colonization from the agar to the model biomaterial was efficiently prevented by the photothermal heating of the AuNRs. However, the control samples were prone to colonization and eventually biofilm formation (Figure 6A−C).

In the development of novel antibacterial surface modifications, it is important that the modifications do not impede the biomaterial's innate properties, like osseointegration for titanium implants, to any significant extent. With the systems

https://doi.org/10.1021/acsanm.5c00324
ACS Appl. Nano Mater. 2025, 8, 3661−3670

studied here, this becomes relevant when considering the load of AuNRs on the surface needed to obtain an antibacterial effect. In the present study, we show a significant antibacterial activity of glass substrates functionalized with around 100 AuNR/μm^2 (14% projected area coverage) against both *S. aureus* and *E. coli*, compared to previous studies where coverages ranging from a few hundred nanoparticles per μm^2 to complete multilayer coatings can be found.[20−23] Using high nanoparticle loadings will not only alter the biomaterial's innate characteristics, but also influence the plasmonic properties of the nanoparticles. Tightly packed or agglomerated AuNRs interact through plasmon coupling, altering their optical properties, and thereby affecting the photothermal efficiency. The well-defined surface-immobilization achieved in this study allowed the AuNRs to retain their optical properties on glass with minimum perturbation by plasmon coupling (Figure 2A), giving potential for high photothermal efficiency, and demonstrating significant antibacterial activity upon NIR illumination at sufficient intensity (Figure 5).

To summarize, this work emphasizes the antibacterial efficacy of surface-immobilized gold nanorods on glass and titanium irradiated with NIR light. Our findings provide new insights into the important influence of the substrate properties for developing photothermal antibacterial biomaterial modifications with surface-immobilized AuNRs and NIR light, and show the potential of the modification strategy for combatting biomaterial-associated infections.

CONCLUSIONS

The development of antibacterial biomaterial modifications is crucial for enhancing the safety and effectiveness of medical treatments involving devices such as implants. In this study, we investigated the antibacterial efficacy of gold nanorods immobilized onto glass and titanium upon irradiation with near-infrared light. A noteworthy difference in the origin of the antibacterial effect between the two materials was found: the effect being attributed to plasmonic heating of the gold nanorods for gold nanorods on glass, and to NIR light absorption by the titanium substrate for gold nanorods on titanium. The developed modification strategy exhibits significant antibacterial activity on glass, against both *S. aureus* and *E. coli*, while only inducing minor alterations to the surface chemistry of the support material, showing promise for retention of the biomaterial's innate properties. These results are pivotal for advancing the design of antibacterial biomaterial modifications based on photothermal therapy using gold nanorods, and for deepening our understanding of the interactions between nanomaterials, biomaterials, and bacteria.

ASSOCIATED CONTENT

Supporting Information

The Supporting Information is available free of charge at https://pubs.acs.org/doi/10.1021/acsanm.5c00324.

Additional experimental details (materials and methods), gold nanorod characterization (dimensions, DLS), additional SEM micrographs of the gold nanorod-functionalized materials, spectra from XPS characterization of gold nanorod-functionalized materials, thermal images of the materials after NIR irradiation, and SEM analysis of samples from the antibacterial activity evaluation (PDF)

AUTHOR INFORMATION

Corresponding Author

Martin Andersson − *Department of Chemistry and Chemical Engineering, Chalmers University of Technology, SE-412 96 Gothenburg, Sweden; Centre for Antibiotic Resistance Research in Gothenburg (CARe), SE-413 45 Gothenburg, Sweden;* orcid.org/0000-0003-1523-4697; Email: martin.andersson@chalmers.se

Authors

Maja Uusitalo − *Department of Chemistry and Chemical Engineering, Chalmers University of Technology, SE-412 96 Gothenburg, Sweden; Centre for Antibiotic Resistance Research in Gothenburg (CARe), SE-413 45 Gothenburg, Sweden;* orcid.org/0000-0001-8421-8899

Gustav Eriksson − *Department of Chemistry and Chemical Engineering, Chalmers University of Technology, SE-412 96 Gothenburg, Sweden;* orcid.org/0009-0001-2330-6227

Mats Hulander − *Department of Chemistry and Chemical Engineering, Chalmers University of Technology, SE-412 96 Gothenburg, Sweden; Centre for Antibiotic Resistance Research in Gothenburg (CARe), SE-413 45 Gothenburg, Sweden;* orcid.org/0000-0003-2921-5438

Complete contact information is available at: https://pubs.acs.org/10.1021/acsanm.5c00324

Author Contributions

The manuscript was written through contributions of all authors. All authors have given approval to the final version of the manuscript.

Funding

The research was funded by the Area of Advance in Materials Science at Chalmers University of Technology and the Knut and Alice Wallenberg Foundation through the Wallenberg Academy Fellow program.

Notes

The authors declare no competing financial interest.

ACKNOWLEDGMENTS

MA acknowledges the support from the Stellenbosch Institute for Advanced Study (STIAS) for their fellowship. This work was performed in part at the Chalmers Material Analysis Laboratory, CMAL. Andreas Schaefer is gratefully acknowledged for help with XPS.

ABBREVIATIONS

AuNR, gold nanorod; NIR, near-infrared; Ti-AuNR, gold nanorod-functionalized titanium; Glass-AuNR, gold nanorod-functionalized glass.

REFERENCES

(1) Zimmerli, W. Clinical Presentation and Treatment of Orthopaedic Implant-Associated Infection. *J. Intern Med.* **2014**, *276* (2), 111−119.

(2) Niinomi, M. Recent Metallic Materials for Biomedical Applications. *Metall. Mater. Trans. A* **2002**, *33*, 477−486.

(3) Pabinger, C.; Lothaller, H.; Portner, N.; Geissler, A. Projections of Hip Arthroplasty in OECD Countries up to 2050. *HIP INT* **2018**, *28* (5), 498−506.

(4) Darouiche, R. O. Device-Associated Infections: A Macroproblem That Starts with Microadherence. *Clin. Infect. Dis.* **2001**, *33* (9), 1567−1572.

(5) Busscher, H. J.; Van Der Mei, H. C.; Subbiahdoss, G.; Jutte, P. C.; Van Den Dungen, J. J. A. M.; Zaat, S. A. J.; Schultz, M. J.; Grainger, D. W. Biomaterial-Associated Infection: Locating the Finish Line in the Race for the Surface. *Sci. Transl. Med.* **2012**, *4* (153), 153rv10.
(6) Arciola, C. R.; Campoccia, D.; Speziale, P.; Montanaro, L.; Costerton, J. W. Biofilm Formation in Staphylococcus Implant Infections. A Review of Molecular Mechanisms and Implications for Biofilm-Resistant Materials. *Biomaterials* **2012**, *33* (26), 5967−5982.
(7) Ribeiro, M.; Monteiro, F. J.; Ferraz, M. P. Infection of Orthopedic Implants with Emphasis on Bacterial Adhesion Process and Techniques Used in Studying Bacterial-Material Interactions. *Biomatter* **2012**, *2* (4), 176−194.
(8) Høiby, N.; Bjarnsholt, T.; Givskov, M.; Molin, S.; Ciofu, O. Antibiotic Resistance of Bacterial Biofilms. *Int. J. Antimicrob. Agents* **2010**, *35* (4), 322−332.
(9) Murray, C. J.; Ikuta, K. S.; Sharara, F.; Swetschinski, L.; Robles Aguilar, G.; Gray, A.; Han, C.; Bisignano, C.; Rao, P.; Wool, E.; Johnson, S. C.; Browne, A. J.; Chipeta, M. G.; Fell, F.; Hackett, S.; Haines-Woodhouse, G.; Kashef Hamadani, B. H.; Kumaran, E. A. P.; McManigal, B.; Achalapong, S.; Agarwal, R.; Akech, S.; Albertson, S.; Amuasi, J.; Andrews, J.; Aravkin, A.; Ashley, E.; Babin, F. X.; Bailey, F.; Baker, S.; Basnyat, B.; Bekker, A.; Bender, R.; Berkley, J. A.; Bethou, A.; Bielicki, J.; Boonkasidecha, S.; Bukosia, J.; Carvalheiro, C.; Castañeda-Orjuela, C.; Chansamouth, V.; Chaurasia, S.; Chiurchiù, S.; Chowdhury, F.; Clotaire Donatien, R.; Cook, A. J.; Cooper, B.; Cressey, T. R.; Criollo-Mora, E.; Cunningham, M.; Darboe, S.; Day, N. P. J.; De Luca, M.; Dokova, K.; Dramowski, A.; Dunachie, S. J.; Duong Bich, T.; Eckmanns, T.; Eibach, D.; Emami, A.; Feasey, N.; Fisher-Pearson, N.; Forrest, K.; Garcia, C.; Garrett, D.; Gastmeier, P.; Giref, A. Z.; Greer, R. C.; Gupta, V.; Haller, S.; Haselbeck, A.; Hay, S. I.; Holm, M.; Hopkins, S.; Hsia, Y.; Iregbu, K. C.; Jacobs, J.; Jarovsky, D.; Javanmardi, F.; Jenney, A. W. J.; Khorana, M.; Khusuwan, S.; Kissoon, N.; Kobeissi, E.; Kostyanev, T.; Krapp, F.; Krumkamp, R.; Kumar, A.; Kyu, H. H.; Lim, C.; Lim, K.; Limmathurotsakul, D.; Loftus, M. J.; Lunn, M.; Ma, J.; Manoharan, A.; Marks, F.; May, J.; Mayxay, M.; Mturi, N.; Munera-Huertas, T.; Musicha, P.; Musila, L. A.; Mussi-Pinhata, M. M.; Naidu, R. N.; Nakamura, T.; Nanavati, R.; Nangia, S.; Newton, P.; Ngoun, C.; Novotney, A.; Nwakanma, D.; Obiero, C. W.; Ochoa, T. J.; Olivas-Martinez, A.; Olliaro, P.; Ooko, E.; Ortiz-Brizuela, E.; Ounchanum, P.; Pak, G. D.; Paredes, J. L.; Peleg, A. Y.; Perrone, C.; Phe, T.; Phommasone, K.; Plakkal, N.; Ponce-de-Leon, A.; Raad, M.; Ramdin, T.; Rattanavong, S.; Riddell, A.; Roberts, T.; Robotham, J. V.; Roca, A.; Rosenthal, V. D.; Rudd, K. E.; Russell, N.; Sader, H. S.; Saengchan, W.; Schnall, J.; et al. Global Burden of Bacterial Antimicrobial Resistance in 2019: A Systematic Analysis. *Lancet* **2022**, *399* (10325), 629−655.
(10) Huang, X.; Jain, P. K.; El-Sayed, I. H.; El-Sayed, M. A. Plasmonic Photothermal Therapy (PPTT) Using Gold Nanoparticles. *Lasers Med Sci* **2008**, *23* (3), 217−228.
(11) Huang, X.; Neretina, S.; El-Sayed, M. A. Gold Nanorods: From Synthesis and Properties to Biological and Biomedical Applications. *Adv. Mater.* **2009**, *21* (48), 4880−4910.
(12) Bar-Ilan, O.; Albrecht, R. M.; Fako, V. E.; Furgeson, D. Y. Toxicity Assessments of Multisized Gold and Silver Nanoparticles in Zebrafish Embryos. *Small* **2009**, *5* (16), 1897−1910.
(13) Connor, E. E.; Mwamuka, J.; Gole, A.; Murphy, C. J.; Wyatt, M. D. Gold Nanoparticles Are Taken up by Human Cells but Do Not Cause Acute Cytotoxicity. *Small* **2005**, *1* (3), 325−327.
(14) Asharani, P. V.; Lianwu, Y.; Gong, Z.; Valiyaveettil, S. Comparison of the Toxicity of Silver, Gold and Platinum Nanoparticles in Developing Zebrafish Embryos. *Nanotoxicology* **2011**, *5* (1), 43−54.
(15) Weissleder, R. A Clearer Vision for in Vivo Imaging. *Nat. Biotechnol.* **2001**, *19*, 316−317.
(16) Huang, X.; El-Sayed, I. H.; Qian, W.; El-Sayed, M. A. Cancer Cell Imaging and Photothermal Therapy in the Near-Infrared Region by Using Gold Nanorods. *J. Am. Chem. Soc.* **2006**, *128* (6), 2115−2120.
(17) Dickerson, E. B.; Dreaden, E. C.; Huang, X.; El-Sayed, I. H.; Chu, H.; Pushpanketh, S.; McDonald, J. F.; El-Sayed, M. A. Gold Nanorod Assisted Near-Infrared Plasmonic Photothermal Therapy (PPTT) of Squamous Cell Carcinoma in Mice. *Cancer Lett.* **2008**, *269* (1), 57−66.
(18) Zhao, Y.; Guo, Q.; Dai, X.; Wei, X.; Yu, Y.; Chen, X.; Li, C.; Cao, Z.; Zhang, X. A Biomimetic Non-Antibiotic Approach to Eradicate Drug-Resistant Infections. *Adv. Mater.* **2019**, *31* (7), 1806024.
(19) Norman, R. S.; Stone, J. W.; Gole, A.; Murphy, C. J.; Sabo-Attwood, T. L. Targeted Photothermal Lysis of the Pathogenic Bacteria, Pseudomonas Aeruginosa, with Gold Nanorods. *Nano Lett.* **2008**, *8* (1), 302−306.
(20) Yang, T.; Wang, D.; Liu, X. Assembled Gold Nanorods for the Photothermal Killing of Bacteria. *Colloids Surf. B Biointerfaces* **2019**, *173*, 833−841.
(21) Zhu, Y.; Ramasamy, M.; Yi, D. K. Antibacterial Activity of Ordered Gold Nanorod Arrays. *ACS Appl. Mater. Interfaces* **2014**, *6* (17), 15078−15085.
(22) Pihl, M.; Bruzell, E.; Andersson, M. Bacterial Biofilm Elimination Using Gold Nanorod Localised Surface Plasmon Resonance Generated Heat. *Mater. Sci. Eng. C* **2017**, *80*, 54−58.
(23) De Miguel, I.; Prieto, I.; Albornoz, A.; Sanz, V.; Weis, C.; Turon, P.; Quidant, R. Plasmon-Based Biofilm Inhibition on Surgical Implants. *Nano Lett.* **2019**, *19* (4), 2524−2529.
(24) Zhao, Y. Q.; Sun, Y.; Zhang, Y.; Ding, X.; Zhao, N.; Yu, B.; Zhao, H.; Duan, S.; Xu, F. J. Well-Defined Gold Nanorod/Polymer Hybrid Coating with Inherent Antifouling and Photothermal Bactericidal Properties for Treating an Infected Hernia. *ACS Nano* **2020**, *14* (2), 2265−2275.
(25) Zhao, Y.-Q.; Xiu, Z.; Wu, R.; Zhang, L.; Ding, X.; Zhao, N.; Duan, S.; Xu, F.-J. A Near-Infrared-Responsive Quaternary Ammonium/Gold Nanorod Hybrid Coating with Enhanced Antibacterial Properties. *Adv Nanobiomed Res* **2022**, *2* (11), 2200111.
(26) Haghighat Bayan, M. A.; Rinoldi, C.; Rybak, D.; Zargarian, S. S.; Zakrzewska, A.; Cegielska, O.; Põhako-Palu, K.; Zhang, S.; Stobnicka-Kupiec, A.; Górny, R. L.; Nakielski, P.; Kogermann, K.; De Sio, L.; Ding, B.; Pierini, F. Engineering Surgical Face Masks with Photothermal and Photodynamic Plasmonic Nanostructures for Enhancing Filtration and On-Demand Pathogen Eradication. *Biomater. Sci.* **2024**, *12* (4), 949−963.
(27) Nicolle, L. E. Catheter Associated Urinary Tract Infections. *Antimicrob. Resist. Infect. Control* **2014**, *3* (1), 23.
(28) Scarabelli, L.; Sánchez-Iglesias, A.; Pérez-Juste, J.; Liz-Marzán, L. M. A "Tips and Tricks" Practical Guide to the Synthesis of Gold Nanorods. *J. Phys. Chem. Lett.* **2015**, *6* (21), 4270−4279.
(29) Diebold, U.; Madey, T. E. TiO2 by XPS. *Surf. Sci. Spectra* **1996**, *4* (3), 227−231.
(30) Greczynski, G.; Hultman, L. The Same Chemical State of Carbon Gives Rise to Two Peaks in X-Ray Photoelectron Spectroscopy. *Sci. Rep.* **2021**, *11*, 11195.
(31) Jana, N. R. Gram-Scale Synthesis of Soluble, near-Monodisperse Gold Nanorods and Other Anisotropic Nanoparticles. *Small* **2005**, *1* (8−9), 875−882.
(32) Liu, M.; Guyot-Sionnest, P. Mechanism of Silver(I)-Assisted Growth of Gold Nanorods and Bipyramids. *J. Phys. Chem. B* **2005**, *109* (47), 22192−22200.
(33) Uusitalo, M.; Strach, M.; Eriksson, G.; Dmytrenko, T.; Andersson, J.; Dahlin, A.; Hulander, M.; Andersson, M. Photothermal Properties of Solid-Supported Gold Nanorods. *Nano Lett.* **2024**, *24* (40), 12529−12535.
(34) Jang, H. K.; Chung, Y. D.; Whangbo, S. W.; Kim, T. G.; Whang, C. N.; Lee, S. J.; Lee, S. Effects of Chemical Etching with Nitric Acid on Glass Surfaces. *J. Vac. Sci. Technol. A: Vac. Surf. Films.* **2001**, *19* (1), 267−274.
(35) Alkilany, A. M.; Nagaria, P. K.; Hexel, C. R.; Shaw, T. J.; Murphy, C. J.; Wyatt, M. D. Cellular Uptake and Cytotoxicity of Gold Nanorods: Molecular Origin of Cytotoxicity and Surface Effects. *Small* **2009**, *5* (6), 701−708.

https://doi.org/10.1021/acsanm.5c00324
ACS Appl. Nano Mater. 2025, 8, 3661−3670

(36) Johnson, P. B.; Christy, R. W. Optical Constants of Transition Metals: Ti, V, Cr, Mn, Fe, Co, Ni, and Pd. *Phys. Rev. B* **1974**, *9* (12), 5056−5070.
(37) Siegfried, T.; Ekinci, Y.; Martin, O. J. F.; Sigg, H. Engineering Metal Adhesion Layers That Do Not Deteriorate Plasmon Resonances. *ACS Nano* **2013**, *7* (3), 2751−2757.
(38) Habteyes, T. G.; Dhuey, S.; Wood, E.; Gargas, D.; Cabrini, S.; Schuck, P. J.; Alivisatos, A. P.; Leone, S. R. Metallic Adhesion Layer Induced Plasmon Damping and Molecular Linker as a Nondamping Alternative. *ACS Nano* **2012**, *6* (6), 5702−5709.
(39) Baffou, G.; Polleux, J.; Rigneault, H.; Monneret, S. Super-Heating and Micro-Bubble Generation around Plasmonic Nanoparticles under Cw Illumination. *J. Phys. Chem. C* **2014**, *118* (9), 4890−4898.

https://doi.org/10.1021/acsanm.5c00324
ACS Appl. Nano Mater. 2025, 8, 3661−3670